İSTANBUL TECHNICAL UNIVERSITY ★ INSTITUTE OF SCIENCE AND TECHNOLOGY

IMAGING OF PERFECTLY CONDUCTING OBJECTS BURIED IN A DIELECTRIC CYLINDER

M.Sc. Thesis by

Oğuz SEMERCİ, B.Sc.

Department : **ELECTRONICS AND COMMUNICATION ENGINEERING**

Programme : **TELECOMMUNICATION ENGINEERING**

JUNE 2008

İSTANBUL TECHNICAL UNIVERSITY ★ INSTITUTE OF SCIENCE AND TECHNOLOGY

IMAGING OF PERFECTLY CONDUCTING OBJECTS BURIED IN A DIELECTRIC CYLINDER

M.Sc. Thesis by

Oğuz SEMERCİ, B.Sc.

(504061329)

Date of Submission : 5 May 2008

Date of Examin : 11 June 2008

Supervisor : Prof. Dr. İbrahim AKDUMAN

Members of the Examining Committee Assoc. Prof. Dr. Ali YAPAR (İ.T.Ü.)

Asst. Prof. Lale Tükenmez ERGENE (İ.T.Ü.)

JUNE 2008

İSTANBUL TEKNİK ÜNİVERSİTESİ ★ FEN BİLİMLERİ ENSTİTÜSÜ

DİELEKTRİK SİLİNDİR İÇİNE GÖMÜLÜ İLETKEN CİSİMLERİN GÖRÜNTÜLENMESİ

YÜKSEK LİSANS TEZİ

Müh. Oğuz SEMERCİ

(504061329)

Tezin Enstitüye Verildiği Tarih : 5 Mayıs 2008
Tezin Savunulduğu Tarih : 11 Haziran 2008

Tez Danışmanı : Prof. Dr. İbrahim AKDUMAN

Diğer Jüri Üyeleri Doç. Dr. Ali YAPAR (İ.T.Ü.)

Yrd. Doç. Dr. Lale Tükenmez ERGENE (İ.T.Ü.)

HAZİRAN 2008

ACKNOWLEDGEMENT

I would like to thank Prof. Dr. Ibrahim Akduman who gave me the opportunity to work under his supervision, for his precious guidance through accomplishing this thesis study.

I would also like to express my gratitude to Assoc. Prof. Dr. Ali Yapar who never hesitated to help me when I needed, for his assistance and scientific contribution to my studies. I am deeply indebted to Prof. Akduman and Prof. Yapar for the motivation they supplied to me with their endless enthusiasm to do scientific research and for being role models for me who will always guide me through my academic career.

I also would like thank to the other members of Electromagnetic Research Group, my dear colleagues Serhat Selçuk Bucak and Onur Mudanyalı and Ece Ercan for their invaluable moral auspices.

And of course I owe my thanks to my parents for their endless support and faith in me.

June 2008 Oğuz SEMERCİ

TABLE OF CONTENTS

LIST OF FIGURES

LIST OF SYMBOLES

$\vec{E}^i$	:	Incident electric field vector
ε_1	:	Permittivity of the dielectric cylinder
ε_0	:	Permittivity of free space
μ_0	:	Permeability of free space
σ	:	Conductivity of the dielectric cylinder
ω	:	angular frequency
k_0	:	wave number of free space
k_1	:	wave number of the dielectric cylinder
u^i	:	incident field
u^0	:	Total field in the absence of the PEC object
u	:	Total field
D	:	Body of the PEC object
∂D	:	Boundary of the PEC object
$f(\phi)$	:	Shape function of the body D
F_M	:	Non-linear operator applying to $f(\phi)$
$H_n^{(1)}$	:	Hankel function of the first kind
J_n	:	Bessel function

IMAGING OF PERFECTLY CONDUCTING OBJECTS BURIED IN A DIELECTRIC CYLINDER

SUMMARY

Reconstruction of the shape and the location of a perfectly conducting objects constitutes one of the basic and important class of problems in inverse scattering theory. Besides the remarkable theoretical aspects, the relevance of this kind of problems is due to fact that they have a large domain of applications including microwave remote sensing, optical system measurements, underwater acoustics or non-destructive testing, only to mention some examples. Accordingly, such problems have been extensively investigated in the open literature and several methods have been developed. In all these works, the methods are developed for the objects located in an homogeneous space or buried in an unbounded media. On the other hand, the body can be located in a bounded medium such as a dielectric sphere or cylinder. Such problems are of importance especially in medical applications. Within this framework, the aim of this paper is to provide a new, simple and fast method to reconstruct the unknown shape of a perfectly conducting object buried in a dielectric circular cylinder. The cylinder is located in an infinite homogeneous space and illuminated by a plane wave of fixed frequency. The method is valid for objects illuminated from a single direction and several directions. The measurements are performed on a circular domain all around the cylinder. In the method presented here, the measured data is analytically continued to the surface of the cylinder by using the single layer potential representation of the scattered field. For the scattered field inside the cylinder, a circle which is assumed to be the minimum circle covering the unknown object that separates the region into two parts is initially determined. In the outer part between the minimum circle and the boundary of the cylinder the scattered field is expressed as a series through the Bessel functions while it is represented in terms of Taylor series in the region between the unknown object and the minimum circle. The use of the boundary conditions reduces the problem to the solution of a nonlinear equation which can be treated by linearizing in the Newton sense. Since the problem is ill-posed, a regularization in the least square sense is also applied. The proposed method is able to provide satisfactory results when the size of the scatterer is comparable to the wavelength.

DİELEKTRİK SİLİNDİR İÇİNE GÖMÜLÜ İLETKEN CİSİMLERİN GÖRÜNTÜLENMESİ

ÖZET

Mükemmel iletken cisimlerin yer ve şekillerinin tespitine ilişkin yöntemler, ters saçılma problemlerinin önemli bir kısımını oluşturmaktadır. Teorik açıdan incelenmeye değer olmalarının yanında, uzaktan algılama, optik sistem ölçümleri, su altı akustiği, tahribatsız muayene gibi önemli uygulama alanlarının mevcut olması, bu tür problemleri önemini arttırmaktadır. Neticede söz konusu problemler literatürde sıklıkla karşımıza çıkmaktadır ve çözümlerinde bir çok farklı yöntem kullanılmıştır. Bu farklı çalışmalarda şekli belirlenecek cismin homojen uzayda ya da sınırlı olmayan bir ortamda gömülü olarak bulunduğu kabul edilmiştir. Ancak, cismin sınırlı bir ortamda, örneğin bir homojen dielektrik slindirin içine gömülü olduğu durum da incelenmeye değerdir. Bu tür problemler özellikle tıbbi uygular için önemlidir. Bu tez çalışmasında, dielektrik silindir içine gömülü mükemmel iletken bir cismin şeklinin belirlenmesine ilişkin yeni, basit ve hızlı bir yöntem tanıtılmıştır. Sınırsız homojen uzayda bulunan dielektrik silindir, tek frekanslı düzlem dalgayla aydınlatılmaltadır. Sunulan metod tek yönden ve çok yönden aydınlatma sonucu elde edilen veriler için geçerlidir. İki durum da ayrı ayrı ele alınacak ve karşılaştırılacaltır. Saçılan alan silindiri çevreleyen dairesel bir domende yapılır ve tek tabakalı potansiyel gösterilimi yardımıyla slindir yüzeyine kadar analitik devam ettirilir. Silindirin içinde ise, yarıçapı bilinmeyen cisiminkinden biraz büyük olacak şekilde bir minimum çember seçilir ve silindirin yüzeyi ile bu minimum daire arasında saçılan alanın Bessel fonksiyonları serisi gösteriliminden yararlanılır. Minimun daire ile mükemmel iletken cisim yüzeyi arasında kalan bölgede ise Taylor açılımından yararlanılarak saçılan alan ifade edilir. Mükemmel iletken cisim yüzeyindeki sınır koşulu yardımıyla elde edilen doğrusal olmayan denklem, bilindik Newton methodu ile doğrusallaştırılıp çözülür. Son olarak minumun kareler yöntemiyle hata azaltılır ve aranan yüzey elde edilir. Sunulan yöntem çalışılan dalga boyu mertebelerindeki cisimlerde iyi sonuçlar vemektedir.

1. INTRODUCTION

In this section a survey of related previous work with brief discussions about different methods is presented before the method proposed in this thesis work is introduced. Additionally, the inverse electromagnetic scattering phenomenon is explained concisely.

Electromagnetic scattering is a physical phenomenon where an electromagnetic incident wave is scattered and the total field at any point in space can be written as the sum of the original incident field and the scattered field, in the presence of an inhomogeneity. The electromagnetic direct scattering problem is the problem of determining the scattered field when the geometrical and physical properties of the scatterer are known. Thus, there many books and papers have been published about scattering of electromagnetic waves [1–5]. On the other hand, inverse scattering is the problem of inferring information on the source of the known scattering field data. Practically, this data is obtained via measurements in a particular domain. However, in order to test the reconstruction algorithms the data can be obtained synthetically by solving the direct problem, which is case in this proposed thesis.

Reconstruction of the shape of a conducting object by using electromagnetic or acoustic waves is one of the fundamental problems of inverse scattering theory not only for its mathematical and physical importance but also for the wide range of applications in the areas of microwave remote sensing, optical system measurements, underwater acoustics and non-destructive testing of materials etc. Additionally, various medical imaging applications are concerned with reconstructing the inhomogeneities by solving the arisen inverse scattering problems. Since 1980's , intensive studies have concerned reconstruction algorithms able to give an efficient solution to quantitative imaging. Spectral methods, based on the so-called diffraction tomography (DT), have been

investigated essentially with applications to ultrasonics or microwaves [6–10]. The main advantages in using such methods are to exhibit explicit formulas for solving the imaging problem and to profit from existing fast numerical algorithms (fast Fourier transform). These algorithms can be implemented on small computers in connection with imaging systems using microwaves or ultrasound [7], [6] for quasi-real time processing purposes.

Another application area of microwave imaging is non-destructive testing(NDT). Several papers have been published proposing methods for NDT applications [11–15], which have wide range of implementation areas including construction and building technology [15]. A very recent paper addresses a methodological approach for detection of cracks on dielectric or conducting objects [12]. In the proposed algorithm, the inverse scattering equations are solved by means of different optimization strategies based on employing parallel and single precesses in order minimize the cost function using a suitable genetic algorithm.

At this point it is worth to emphasize that, implementing genetic algorithms on microwave imaging techniques is widely investigated [11–17] since they are versatile and allow optimization on complex multi-modal search spaces [18]. In 1998, Qing [14] published a paper proposing a method to solve the electromagnetic inverse scattering problem of 2-D perfectly conducting targets by using the real-coded genetic algorithm. Later, realizing that the local shape functions defining the surface of the conducting object can not be properly approximated by trigonometric series he published another paper in which using of B-splines is proposed [13]. In these papers, the inverse problem is reduced to an optimization one with the location parameters and the coefficients of the local shape functions (either trigonometric series coefficients or closed cubic B-splines control points) as optimization parameters. Using real-coded genetic algorithms provides good results, however they constitute extreme time consumption

Another widely used reconstruction algorithm is linear sampling, which is first proposed in 1996 by Colton and Kirsh [19]. In this paper the method was used to reconstruct 2D obstacles using Dirichlet and Neumann boundary conditions in a inhomogeneous media. Later in 1998 Colton and Monk [20] published a paper addressing a fast microwave imaging method for detection of leukemia by

determining the aberrant inhomogeneities in the cross-section of a bone marrow indicating a possible presence of a tumor. Different work proposing possible practical application areas for the method such as impedance tomography [21], elasticity [22] and detection of buried objects [23] published in the following years.

Depending on the practical purpose, inverse problems can be solved for different geometries. According to the physical configuration, the object may be assumed to be located in an infinite host medium or in a layered one. Several methods based on different approaches such as physical optics theory, Newton-Kantorovich method, equivalent source technique, and decomposition methods have been developed in the case of infinite host medium [24–27]. Although, Newton-Kantarovitch method [28] gives good results it needs a good initial guess for reliable reconstructions. Unfortunately, such a priori knowledge is not always available in practical applications. Some of these methods have also been applied for the shape reconstruction of objects buried in a half-space or in plenarily layered medium [29], [30]. The latter one has many practical applications such as mine detection, nondestructive testing of pipelines etc. As well as, a method for reconstruction of inhomogeneous materials coated on a conductor of a known shape had been developed [31], [32]. By comparing these two groups of problems it can be observed that the background medium has a strong effect on the reconstruction algorithms since the scattering phenomenon becomes more complicated.

Within this framework another interesting problem would be the imaging of conducting objects located in a cylindrically layered medium which is not widely investigated in the open literature as far as we know. Such a problem may have potential applications in nondestructive testing of coated conducting structures. It would also be worth to analyze this problem to understand the effect of cylindrically layered media on the imaging algorithms. Along this line the main aim of this paper is to give a simple and fast method for the reconstruction of the shape of a PEC object located into a cylindrical dielectric region. To this aim the object is illuminated by a time harmonic plane wave with a fixed frequency and the scattered field is measured in the far field region. The method is based on a special representation of the scattered field in the whole space. This

representation first allows one to continue the far field data analytically to the boundary of the dielectric cylinder. Then the field inside the dielectric cylinder is expressed as a series of cylindrical harmonics whose coefficients are calculated simply applying the boundary conditions on the cylinder surface. Note that this representation will only be valid to the boundary of a fictitious minimum circle covering the unknown scatterer due to the discontinuity in the angular direction. To overcome this difficulty the field inside the minimum circle is expressed as a Taylor expansion of the series representation. Final step of the method is to obtain a non-linear equation in terms of the unknown surface function which is solved iteratively by well known Newton algorithm.

The thesis is organized as follows. In Chapter 2 the exploited representations of the scattered field are recalled and discussed, and the solution of the linear inverse problem arising from the single-layer potential equation is addressed. Then, in Chapter 3 the reconstruction algorithm is outlined and the details on the adopted Newton's scheme are given. Implementation of multi illuminations is discussed and formulated in Chapter 4. And finally, Chapter 5 reports the implementation of the proposed method and several numerical examples which show that the method yields satisfactory reconstructions for convex and concave surfaces. Conclusion follows.

2. A SPECIAL REPRESENTATION OF THE SCATTERED FIELD

Consider the two-dimensional scattering problem illustrated in Figure 2.

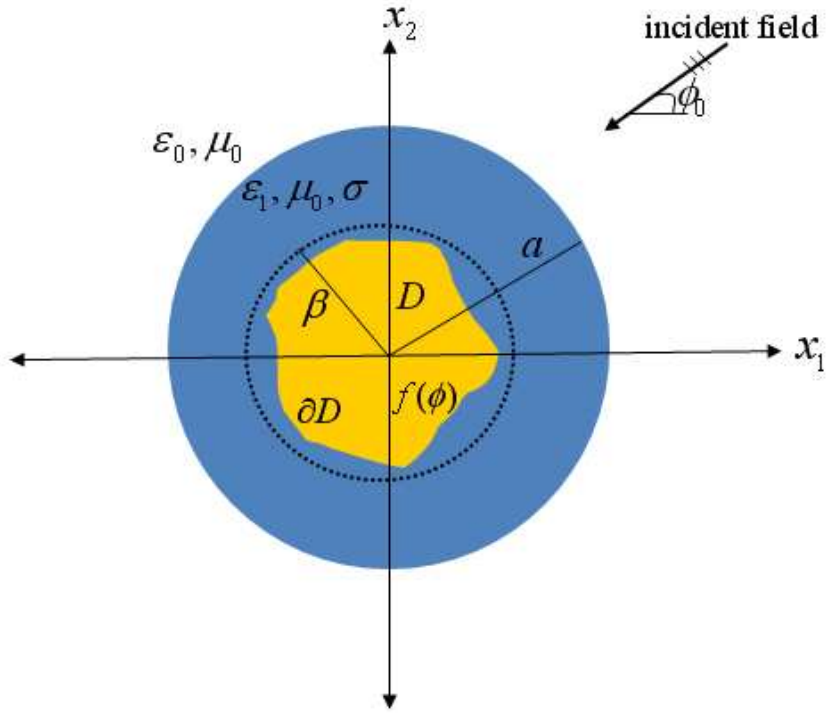

Figure 2.1: Geometry of the problem

In this configuration, D is a perfectly electric conducting (PEC) cylindrical body whose boundary ∂D is defined by the parametric equation $x_1 = x_1(t)$, $x_2 = x_2(t)$, $t \in (0, 2\pi)$. Note that ∂D can also be defined via polar equation of the form $\rho = f(\phi)$, $\phi \in (0, 2\pi)$ where (ρ, ϕ) are the cylindrical polar coordinates, and in the following we will assume that D has a star-like shape. The body D is located in a homogeneous circular cylinder with radius a whose electromagnetic constitutive parameters are ε_1, μ_0 and σ.

The surrounding medium outside the circular dielectric region is assumed to be free space. The inverse scattering problem considered here consists in recovering the shape of the body D, i.e., the function $f(\phi)$, from a set of far field measurements of the scattered wave. To this aim, the homogeneous cylinder is

illuminated by a time-harmonic plane wave whose electric field vector $\vec{E}^i$ is always parallel to the Ox_3 axis. By assuming and omitting the time factor $\exp(-i\omega t)$, this field is given by:

$$\vec{E}^i = (0,0,u^i(\rho,\phi)) \tag{2.1}$$

with

$$u^i(\rho,\phi) = e^{-ik_0\rho\cos(\phi-\phi_0)} \tag{2.2}$$

where ϕ_0 is the incidence angle and $k_0 = \omega\sqrt{\varepsilon_0\mu_0}$ is the wave number of free space. Due to the homogeneity in the x_3 direction, the total electric field vector will have only x_3 component, i.e.; $\vec{E} = (0,0,u(\rho,\phi))$, thus the problem is reduced to a scalar one in terms of $u(\rho,\phi)$). In order to formulate the problem in a more appropriate way the total field is decomposed as $u = u^0 + u^s$, with

$$u^0 = \left\{ \begin{array}{ll} \sum\limits_{n=-\infty}^{\infty} [(-i)^n J_n(k_0\rho) + K_n H_n^{(1)}(k_0\rho)]e^{in(\phi-\phi_0)} & ,\rho > a \\ \sum\limits_{n=-\infty}^{\infty} L_n J_n(k_1\rho)e^{in(\phi-\phi_0)} & ,\rho < a \end{array} \right\} \tag{2.3}$$

stands for the total electric field in the absence of the conducting body D. The unknown coefficients K_n and L_n can be determined using Dirichlet and Neumann boundary conditions on the surface of the dielectric cylinder as,

$$u^0(\rho \to a^+,\phi) = u^0(\rho \to a^-,\phi) \tag{2.4}$$

and

$$\frac{\partial u^0(\rho \to a^+,\phi)}{\partial \rho} = \frac{\partial u^0(\rho \to a^-,\phi)}{\partial \rho} \tag{2.5}$$

multiplying both sides of each equation by $e^{-im\phi}$ and integrating over one period, equations (2.4) and (2.5) gives

$$(-i)^m J_m(k_0 a) + K_m H_m^{(1)}(k_0 a) = L_m J_m(k_1 a) \tag{2.6}$$

$$(-i)^m J'_m(k_0 a) + K_m H'^{(1)}_m(k_0 a) = L_m J'_m(k_1 a) \tag{2.7}$$

where $\prime$ denotes the derivative of the bessel functions with respect to the radial direction ρ. The unknown coefficients K_n and L_n are immediately obtained from (2.6) and (2.7) as

$$K_n = \frac{(-i)^n J_n'(k_0 a) J_n(k_1 a) - (-i)^n J_n(k_0 a) J_n'(k_1 a)}{H_n^{(1)}(k_0 a) J_n'(k_1 a) - J_n(k_1 a) H_n'^{(1)}(k_0 a)} \tag{2.8}$$

$$L_n = \frac{-(-i)^n J_n'(k_0 a) H_n^{(1)}(k_0 a) + (-i)^n J_n(k_0 a) H_n'^{(1)}(k_0 a)}{H_n'^{(1)}(k_0 a) J_n(k_1 a) - J_n'(k_1 a) H_n^{(1)}(k_0 a)}. \tag{2.9}$$

in which J_n and $H_n^{(1)}$ are the Bessel and the Hankel function of the first kind with order n, respectively.

Then the scattered field, $u^s(\rho,\phi)$, which corresponds to the contribution of the body D to the total field can be expressed by a special representation inside and outside the circular cylinder. For the region $\rho > a$ it is convenient to represent the scattered field as a single layer potential [33] in the form

$$u^s(\rho,\phi) = \frac{i}{4}\int_0^{2\pi} H_0^{(1)}(k_0\sqrt{\rho^2+a^2-2\rho a\cos(\phi-\tau)}\,)\psi(\tau)ad\tau, \quad \rho > a. \tag{2.10}$$

Here $H_0^{(1)}$ denotes the Hankel function of the first kind with zero order and ψ is the unknown density function. In order to find an appropriate expression for the scattered field inside the circular cylinder, we consider a circle with radius $\rho = \beta, \quad \beta > max(f(\phi)$, (see figure1) that separates the space outside the object and inside the circular cylinder into two regions. This circle is assumed to be close to the minimum circle covering the object D and in the following a (possibly approximated) knowledge of its radius is assumed. Now in the region $\rho \in (\beta, a)$ the scattered field can be written in terms of cylindrical harmonics as follows

$$u^s(x) = \sum_{n=-\infty}^{\infty}\Big[A_n H_n^{(1)}(k_1\rho) + B_n J_n(k_1\rho)\Big]e^{in\phi}, \quad \rho \in (\beta, a) \tag{2.11}$$

where A_n and B_n are unknown coefficients to be determined. Note that this representation is not valid in the region $\rho < maxf(\phi)$ since there are physical discontinuities in the angular direction ϕ. For a representation of the scattered field in the interior region $f(\phi) < \rho < \beta$ one can use Taylor formula around the

circle $\rho = \beta$, that is,

$$u^s(\rho,\phi) = \sum_{m=0}^{M} \frac{1}{m!} \frac{\partial^m u^s(\beta,\phi)}{\partial \rho^m} (\rho-\beta)^m + R_M(\rho,\phi), \quad \rho \in (f(\phi),\beta] \tag{2.12}$$

with the remainder term

$$R_M(\rho,\phi) = \frac{1}{M!} \int_{\beta}^{\rho} (\rho-\rho')^M \frac{\partial^{M+1} u(\rho',\phi)}{\partial \rho'^{M+1}} \, d\rho'. \tag{2.13}$$

The m^{th} order derivative of u^s appearing in (2.12) can be calculated from (2.11) as

$$\frac{\partial^m u^s(\beta,\phi)}{\partial \rho^m} = \sum_{n=-\infty}^{\infty} \frac{\partial^m}{\partial \rho^m} \left[A_n H_n^{(1)}(k_1\rho) + B_n J_n(k_1\rho) \right] \Big|_{\rho=\beta} e^{in\phi} \tag{2.14}$$

As a result the scattered field u^s is now represented in the whole space by the equations (2.10), (2.11) and (2.12). This representation together with boundary conditions can now be used for the solution of both direct and inverse scattering problems. In the next section an iterative algorithm is described which is based on the Newton method for the solution of the inverse problem.

3. SOLUTION OF THE INVERSE PROBLEM

In the inverse scattering problem considered here, the scattered field is assumed to be known on the far field region. Taking the asymptotic behavior of the Hankel function into account in (2.10) the far field pattern of the scattered field can be written as

$$u_\infty^s(\hat{x}) = \frac{e^{i\pi/4}}{\sqrt{8\pi k_0}} \int_0^{2\pi} e^{-ik_0\rho\cos(\tau-\theta)} \psi(\tau) a d\tau \tag{3.1}$$

where $\hat{x} = (\cos\theta, \sin\theta)$ is the observation direction. (3.1) can be rearranged in an operator equation form as follows:

$$A\psi = u_\infty^s(\hat{x}) \tag{3.2}$$

where the integral operator A is defined by

$$A\psi = \frac{e^{i\pi/4}}{\sqrt{8k_0\pi}} \int_0^{2\pi} e^{-ik_0 a\cos(\tau-\theta)} \psi(\tau) a d\tau. \tag{3.3}$$

The operator A has an analytic kernel and therefore the equation (3.2) is ill-posed. For this reason, some kind of regularization has to be applied and only an approximation of the sought function ψ can be achieved [33, 34]. Here we apply a regularization in the Tikhonov sense and solve the unknown density function as

$$\psi = (\alpha I + A^* A)^{-1} A^* u_\infty^s, \tag{3.4}$$

where I is the identity operator and A^* is the adjoint of the operator A. The scattered field u^s is now known outside the region $\rho > a$ by the aid of the equations (2.10) and (3.4). In order to obtain the field in the region $\rho \in (f(\phi), a)$ it is obvious that one has to calculate the unknown coefficients A_n and B_n appearing in (2.11). To this aim first define the finite Fourier transform of the scattered field as

$$\hat{u}^s(\rho, n) = \int_0^{2\pi} u^s(\rho, \phi) e^{-in\phi} d\phi \tag{3.5}$$

Now using the boundary conditions

$$u_s(\rho = a+0, \phi) = u_s(\rho = a-0, \phi) \tag{3.6}$$

$$\frac{\partial u_s}{\partial \rho}(\rho = a+0, \phi) = \frac{\partial u_s}{\partial \rho}(\rho = a-0, \phi) \tag{3.7}$$

the following system of equations can be obtained for the coefficients A_n and B_n

$$H_n^{(1)}(k_1 a)A_n + J_n(k_1 a)B_n = \hat{u}^s(a,n) \tag{3.8}$$

$$H_n'^{(1)}(k_1 a)A_n + J_n'(k_1 a)B_n = \hat{u}^{s\prime}(a,n) \tag{3.9}$$

The solution of the (3.8) and (3.9) reads

$$A_n = \frac{-\hat{u}^s(a,n)J_n{}'(k_1 a) + \hat{u}^{s\prime}(a,n)J_n(k_1 a)}{J_n{}'(k_1 a)H_n^{(1)}(k_1 a) + J_n(k_1 a)H_n'^{(1)}(k_1 a)} \tag{3.10}$$

$$B_n = \frac{\hat{u}^s(a,n)H_n'^{(1)}(k_1 a) - \hat{u}^{s\prime}(a,n)H_n^{(1)}(k_1 a)}{-J_n'(k_1 a)H_n^{(1)}(k_1 a) + J_n(k_1 a)H_n'^{(1)}(k_1 a)} \tag{3.11}$$

The final step for the solution of the inverse problem is to apply the boundary condition on the boundary of D which states that the total field must vanish on ∂D:

$$u(\rho, \phi) = 0, \qquad \rho = f(\phi). \tag{3.12}$$

Using (2.12) and (2.3) the explicit expression of the this boundary condition can be written as

$$u^0(f(\phi), \phi) + \sum_{m=0}^{M} \frac{1}{m!} \frac{\partial^m u^s(\beta, \phi)}{\partial \rho^m} (f(\phi) - \beta)^m = 0. \tag{3.13}$$

(3.13) is a non-linear equation in terms of the unknown surface variation $f(\phi)$ and it can be rewritten in a compact form as follows:

$$F_M(f) = 0 \tag{3.14}$$

where F_M is the non-linear operator given by

$$F_M(f) = \sum_{m=0}^{M} c_m \left(\frac{\rho - \beta}{\lambda} \right)^m = 0. \tag{3.15}$$

Note that, for given data, the coefficients c_m in (3.15) are all known through the relation (2.14). Thus the reconstruction problem is reduced to the solution of non-linear equation (3.14) for the unknown function f.

The accuracy of the Taylor series in (2.12) (neglecting the remainder for $\rho = f(\phi)$) is related to $\left|\frac{\rho-\beta}{\lambda}\right|$, which is the distance between the surface ∂D and the circle $\rho = \beta$ for a certain ϕ. If the circle $\rho = \beta$ is close to the surface (with respect to the wavelength) and the surface function $f(\phi)$ is a slightly varying one, the distance $|f(\phi) - \beta|$ becomes small. Therefore, provided that the above condition (which entails some limitations on the angular variability of the unknown profiles) is fulfilled, the number M which is nothing but the truncation number of the series (2.12) can be small. To select the appropriate M, a threshold value δ is chosen and the series (2.12) is truncated at the smallest M satisfying

$$\left| c_M (\min[f(\phi)] - \beta)^M \right| < \delta. \tag{3.16}$$

As this expression would require a knowledge of $f(\phi)$, which is the unknown of the problem, from a practical point of view we achieve an estimate of M by substituting $min[f(\phi)] = a/2$ into (3.16).

The non-linear equation (3.14) is solved iteratively via Newton method [35]. Hence, for an initial guess f_0, the non-linear equation (3.14) is replaced by the linearized equation

$$F_M(f_0) + F'_M(f_0)\Delta f = 0 \tag{3.17}$$

where $\Delta f = f - f_0$, that needs to be solved for Δf in order to improve an approximate boundary ∂D given by the function f_0 into a new approximation with surface function $f_0 + \Delta f$. In (3.17) F'_M denotes the Frechet derivative of the operator F_M with respect to f. It can be shown that F'_M reduces to the ordinary derivative of F_M with respect to f.

The Newton method consists in iterating this procedure, i.e.: in solving

$$F'_M(f_i)\Delta f_{i+1} = -F_M(f_i), \quad i = 0,1,2,3,.... \tag{3.18}$$

for Δf_{i+1} to obtain a sequence of approximations through $f_{i+1} = f_i + \Delta f_{i+1}$.

As this solution will be sensitive to errors in the derivative of F_M in the vicinity of zeros, a finite dimensional approximation of Δf is looked for in order to obtain a stable procedure. In particular, the approximated solution is expressed in terms of a linear combination of some basis functions $\vartheta_p(\phi)$, $p = 1,\ldots,P$, as

$$\Delta f(\phi) = \sum_{p=1}^{P} a_p \vartheta_p(\phi). \tag{3.19}$$

Then (3.17) is satisfied in the least squares sense, that is, the coefficients $a_1,\ldots,a_P$ in (3.19) are determined so that for a set of grid points $\phi^1,\ldots,\phi^J$ the sum of squares

$$\sum_{j=1}^{J} \left| F'_M(f(\phi^j)) \sum_{p=1}^{P} a_p \vartheta_p(\phi^j) + F_M(f(\phi^j)) \right|^2 \tag{3.20}$$

is minimized.

The number of basis functions P in (3.19) can be considered as a further regularization parameter. As a matter of fact, choosing P too large may lead to instabilities due to the ill-posedness of the underlying inverse problem, while choosing P too small would result in poor approximation quality. On the other hand, a reduction of the number P of unknown coefficients has a beneficial effect in reducing occurrence of false solutions, which may arise due to the non-linearity of the problem. Hence, one has to compromise between stability and accuracy and in this sense P serves as a regularization parameter.

4. MULTIPLE ILLUMINATION CASE

In order to achieve less erroneous and more effective reconstructions, a common idea is to use multiple illuminations [36]. Thus, the method proposed can be upgraded to use data which is obtained through different experiments or simulations made with different incidence angles.

For this aim the object is illuminated from different angles non-simultaneously and each data is analytically continued leading a polynomial equation as explained in Chapter 3. As the polynomial equation which is expressed in a compact operator form in (3.13) changes with the illumination angle, the resulting compact operator for n^{th} illumination can be expressed as

$$F_M^n(f) = \sum_{m=0}^{M} c_m^n \left(\frac{\rho - \beta}{\lambda} \right)^m = 0. \tag{4.1}$$

Knowing that the unknown surface function f is independent of the illumination angle, a system of non-linear equations consisting of resulting polynomial equations obtained from N different illuminations can be constructed as

$$\begin{aligned} F_M^1(f) &= 0 \\ &\vdots \\ F_M^n(f) &= 0 \end{aligned} \tag{4.2}$$

The non-linear system is solved via Gauss-Newton method. In particular, given an initial guess f_0, the system in (4.3) which is the linearization of (4.2) is solved iteratively.

$$\begin{pmatrix} F_M^{1'}(f_i) \\ \vdots \\ F_M^{N'}(f_i) \end{pmatrix} \Delta f_{i+1} = - \begin{pmatrix} F_M^1(f_i) \\ \vdots \\ F_M^N(f_i) \end{pmatrix} \tag{4.3}$$

where f_i denotes the estimated shape at the i^{th} iteration and the updated shape is found by $f_{i+1} = f_i + \Delta f_{i+1}$. Here $F_M^{n'}$ indicates the Frechet derivative of F_M^n with

respect to f_i. The Frechet derivative seen in (4.3) reduces to ordinary derivative since F_M^n are polynomials of f_i. Similar to the single illumination case, the solution of the linear system (4.3) is sensitive to errors in the derivative of F_M^n. Solving this system of equations in the least square sense is a reliable approach to deal with this obstacle. Particularly, the term Δf_{i+1} is expanded into a series of $2K+1$ trigonometric polynomials as:

$$\Delta f_{i+1} = \sum_{k=0}^{K} a_k^{(i+1)} cos(k\phi) + \sum_{1}^{K} b_k^{(i+1)} sin(k\phi) \tag{4.4}$$

where $a_k^{(i+1)}$ and $b_k^{(i+1)}$ are the coefficient to be determined at $(i+1)^{th}$ iteration. Next, substituting (4.4) in (4.3) and discretizing ϕ into Q different points the system in (4.3) is recasted in a matrix equation form as:

$$J_F(f_i)x_{i+1} = -V(f_i) \tag{4.5}$$

Solving (4.5) in the least square sense gives the solution given in (4.6).

$$x_{i+1} = -[J_F^*(f_i)J_F(f_i)]^{-1}J_F^*(f_i)V(f_i) \tag{4.6}$$

Here, $(N \times Q) \times 1$ column vector V consists of different values of F_M at Q collocation points. Whereas, $(N \times Q) \times (2K+1)$ matrix J_F^* denotes the projection of the matrix F' over the trigonometric basis functions and J_F^* denotes it's adjoint. Column vector x_{i+1} contains $(2k+1)$ unknown coefficients in (4.4).

Having found the unknown coefficients, Δf_{i+1} is obtained and iteration process is continued untill the condition $\| x_{i+1} - x_i \| < \delta$ is satisfied for a fixed value of δ.

5. NUMERICAL IMPLEMENTATION AND EXAMPLES

In this section, some numerical results which demonstrate the validity and effectiveness of the method will be provided. Additionally, in each section effects of some parameters as frequency, noise level as well as the properties of the homogeneous cylinder in which the perfectly conducting object is buried, to the reconstruction will be demonstrated. And the last section is devoted to examples which demonstrate the improvements in the quality of reconstructions by using multiple illumination approach. Concise interpretations of the obtained results are made at the end of each section. The scattered field data is synthetically generated by solving the associated forward problem through the mixed double and single-layer potential approach in $J = 150$ discrete points [33]. In all examples, a random term $n_l|u_m^s|e^{2ir_d\pi}$ is added to each scattered field value u_m^s, n_l being the noise level and r_d a random number between 0 and 1. In the application of the least squares solution the basis functions are chosen as $\vartheta_q(\phi) = e^{-iq\phi}, \quad q = 0, \pm 1, ... \pm Q$, wherein, being the unknown function real valued, the corresponding ϑ_q coefficients are enforced to satisfy the Hermitianity condition. Note $P = (2 \times Q + 1)$ in (3.19).

The quality of the estimated shape $\hat{f}$ is quantified by the reconstruction error defined as:

$$err = \sqrt{\frac{\sum_{j=1}^{J} |f(\phi^j) - \hat{f}(\phi^j)|^2}{\sum_{j=1}^{J} |f(\phi^j)|^2}}. \tag{5.1}$$

In the inversion step of the method, the estimated field is used to build the non-linear functional (3.20) and the Newton minimization is performed. In each example the illumination angle, noise level and the number of terms in the Taylor expansion representation are, $\phi_0 = 0$, $n_l = 5\%$ and $M = 5$ unless other values

are specified. The minimum circle is used as the starting guess of the iteration procedure.

5.1 Effect of The Relative Permittivity of The Dielectric Cylinder

In this section the effect of the relative permittivity of the dielectric cylinder is demonstrated. For this aim, a potato shaped object with a radius of 0.3λ buried in a homogeneous dielectric cylinder with a radius and conductivity of 0.4λ and $\sigma = 10^{-2}(S.m^{-1})$ respectively, is considered. The parametric equation of the potato-shaped object is given by

$$x_1 = (0.25 + 0.05\cos 2\phi)\cos\phi$$

$$x_2 = (0.25 + 0.05\sin 4\phi)\sin\phi,\ \phi \in (0, 2\pi).$$

Number of basis functions in the least square regularization is $Q = 8$. Exact and reconstructed shapes for a cylinder with relative dielectric permittivity of $\varepsilon_r = 4$ and $\varepsilon_r = 8$ are given in Figure 5.1 and Figure 5.2. The Reconstruction error for these examples are 6% and 8.5%. For the purpose of showing the robustness of the method, the noise-free case is also considered for $\varepsilon_r = 8$. Figure 5.3 shows the reconstruction with an error of 8%. As it can be observed, the exact and reconstructed shapes are in good agreement in the illuminated part of the object while, due to the introduced regularization, it is smoothed in the non-convex regions. However, satisfying reconstruction of the non illuminated part is also achieved. And the method is quite robust against noise , as it is confirmed by comparison with the noise-free reconstruction.

5.2 Effect of The Thickness of The Dielectric Cylinder

In order to illustrate the effect of the thickness of the dielectric cylinder to reconstruction, it's radius is increased to 0.5λ while other parameters as permittivity and conductivity of the cylinder and number of basis functions used in the least square regularization remained the same. As seen from Figure 5.4 reconstruction is achieved more erroneous (i.e. 11%) for the case that a is increased to 0.5λ. The method is sensitive to increases in the radius of

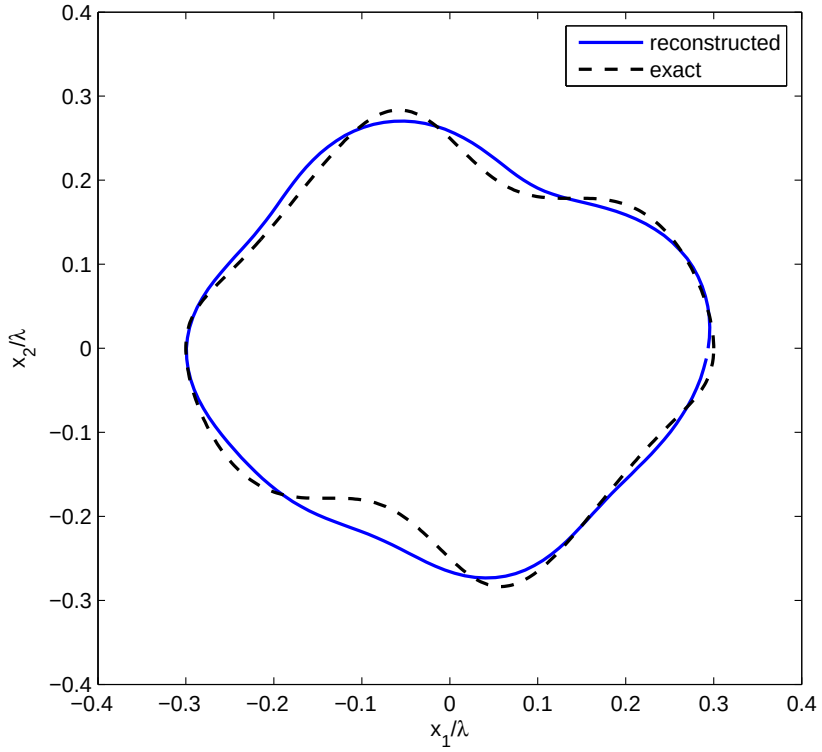

Figure 5.1: Exact and reconstructed geometries of a potato-shape object for $\varepsilon_r = 4$

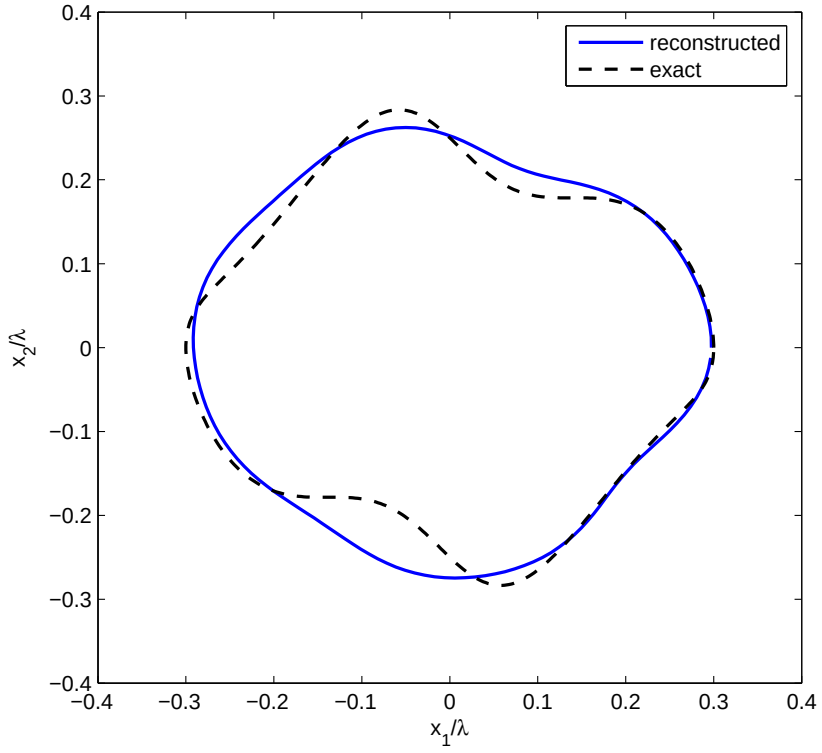

Figure 5.2: Exact and reconstructed geometries of a potato-shape object for $\varepsilon_r = 8$

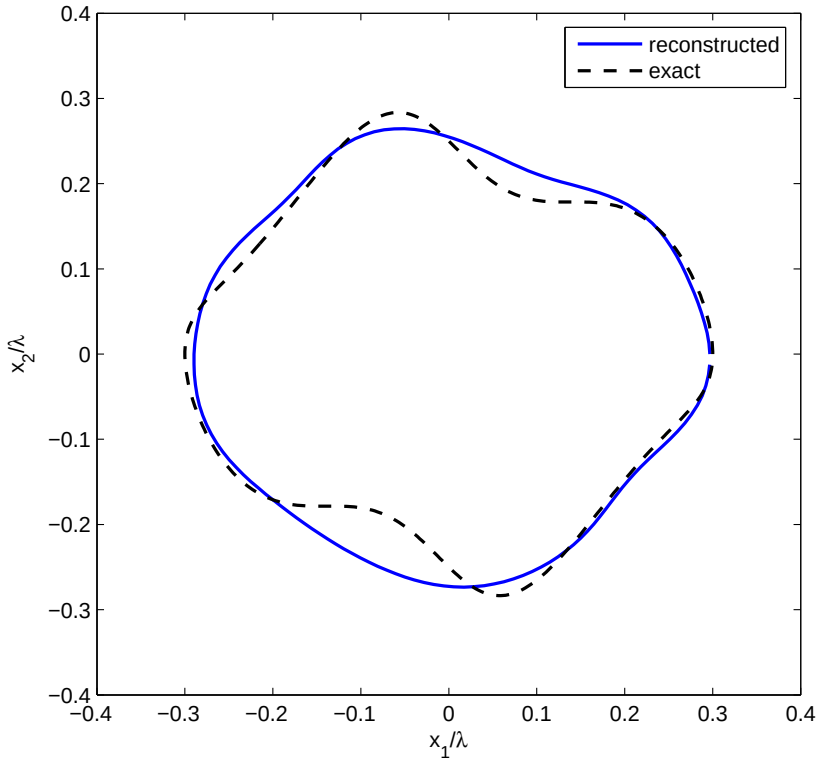

Figure 5.3: Exact and reconstructed geometries of a potato-shape object for $\varepsilon_r = 8$. Noise-free case.

the dielectric cylinder which prevents proper reconstructions for thick coatings compared to the size of the PEC object.

5.3 Effect of The Operating Frequency

For the next examples, operating frequency is increased to $600MHz$. Hence, the radius of the potato-shaped object to be reconstructed relatively increased to 0.6λ. Reconstructions with errors of 21.6% and 7% obtained for $a = 0.8\lambda$ and $a = 0.7\lambda$ are shown in the Figure 5.5 and 5.6. Relative permittivity and conductivity of the cylinder and number of basis functions in the least square regularization is taken $\varepsilon_r = 4$, $\sigma = 10^{-2}(S.m^{-1})$ and $Q = 8$ in order to make consistent comparisons with previous examples. As seen from Figure 5.5 the method leads to acceptable reconstructions if the radius or the coating homogeneous cylinder is not greater than, approximately a wavelength λ.

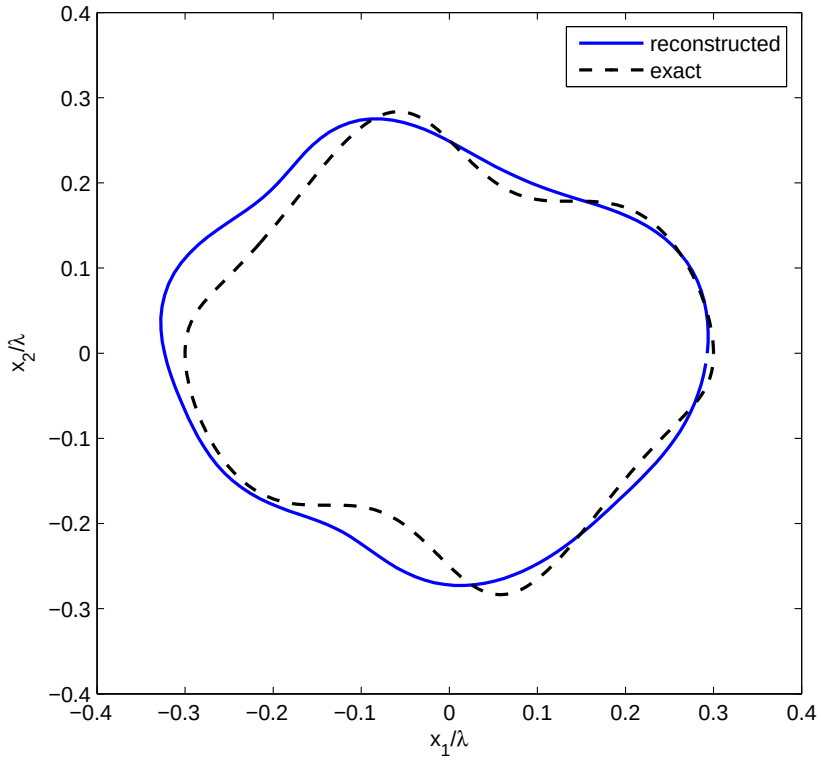

Figure 5.4: Exact and reconstructed geometries of a potato-shape object for $a = 0.5\lambda$

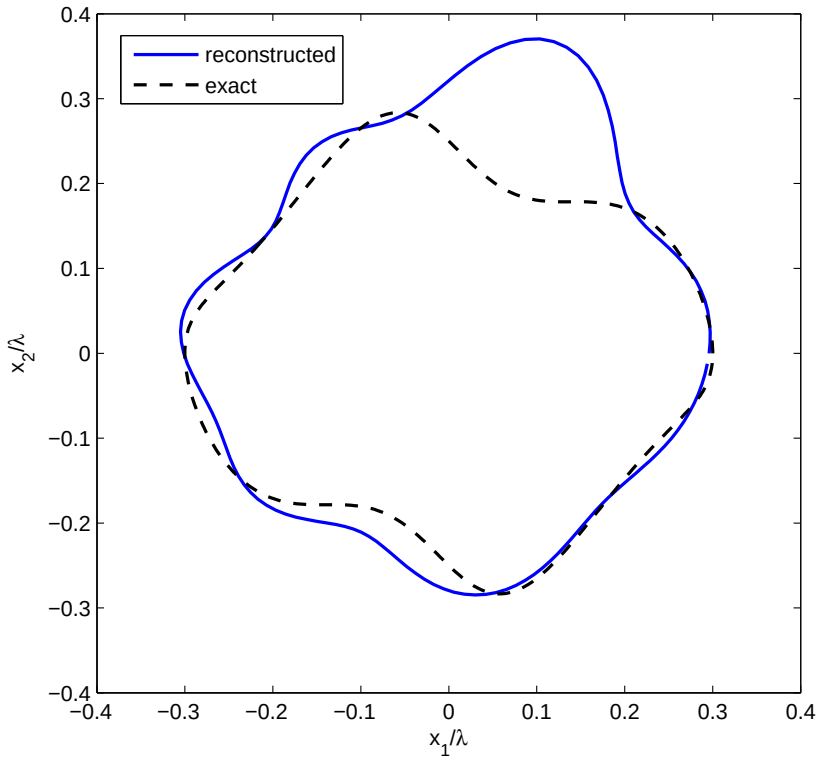

Figure 5.5: Exact and reconstructed geometries of a potato-shape object for $f = 600MHz$ and $a = 0.8\lambda$

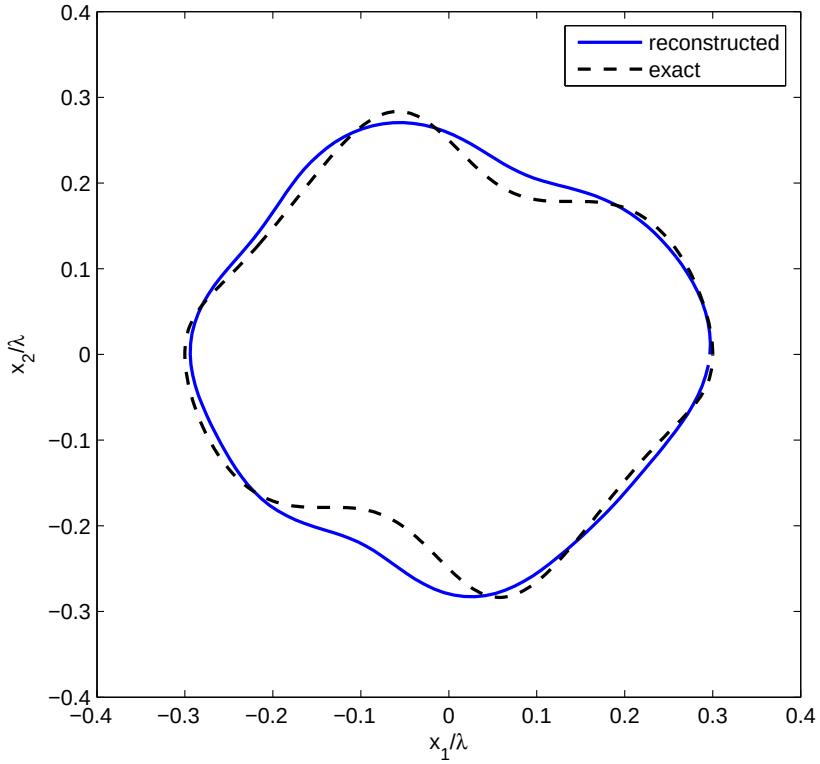

Figure 5.6: Exact and reconstructed geometries of a potato-shape object for $f = 600MHz$ and $a = 0.7\lambda$

5.4 Effect of The Radius of the β Circle

The proposed method requires an approximate knowledge of the radius of the buried PEC object, since Taylor series representation of the scattered field is used between the β circle and the surface of the PEC object. Hence a rough guess of the radius of the β circle is crucial for proper reconstructions. In order the method to be practically reliable, one can expect a good reconstruction to be achieved for a β circle with a radius satisfyingly bigger than the maximum radius of the PEC object. The following examples demonstrate the validity of the method regarding the radius of the β circle compared to maximum radius of the object to be reconstructed. For Figure 5.7 trough Figure 5.9 operating frequency is $300MHz$ while thickness and the permittivity of the dielectric cylinder is taken $a = 0.4$, $\varepsilon_r = 4$ respectively. $Q = 9$ basis functions are used in least square solution. Figures 5.7, 5.8 and 5.9 shows exact and reconstructed geometries with errors of 6%, and 7.5% respectively. It is observed that the method gives satisfactory

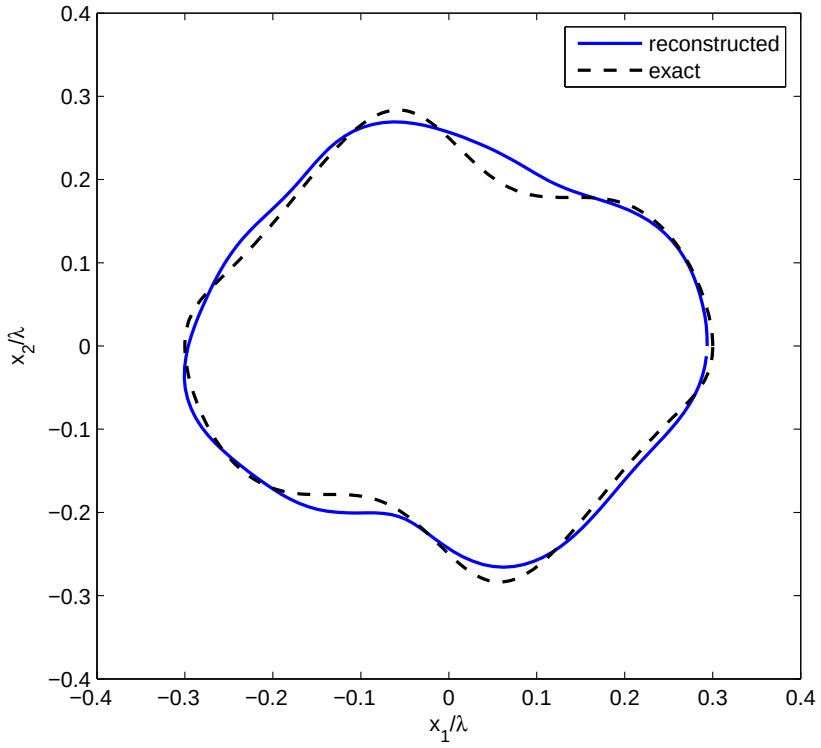

Figure 5.7: Exact and reconstructed geometries of a potato-shape object for the radius of the β is 10% greater than f_{max}

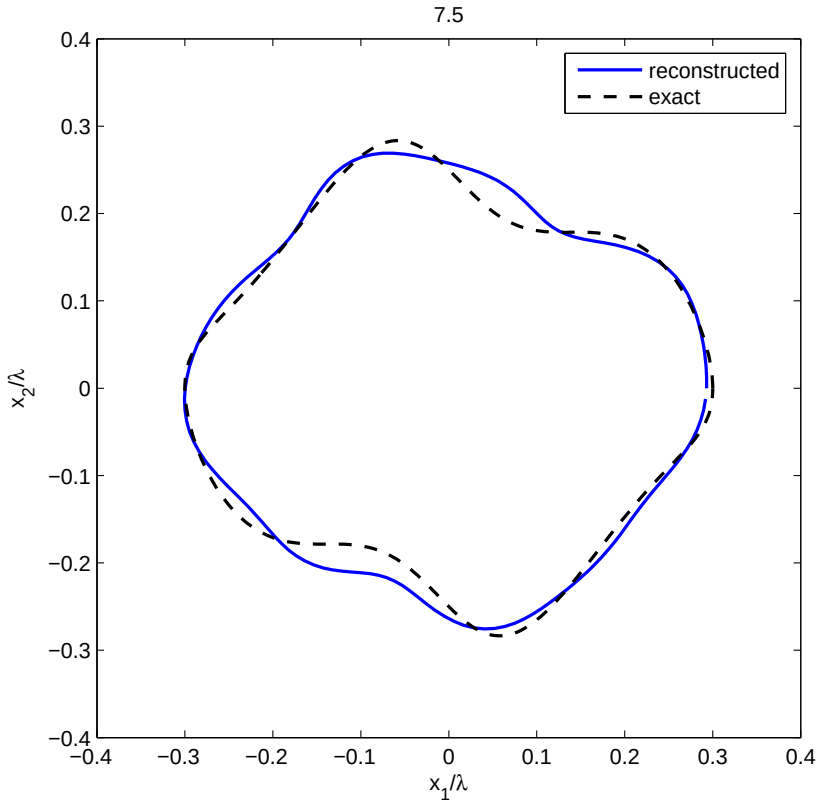

Figure 5.8: Exact and reconstructed geometries of a potato-shape object for the radius of the β is 20% greater than f_{max}

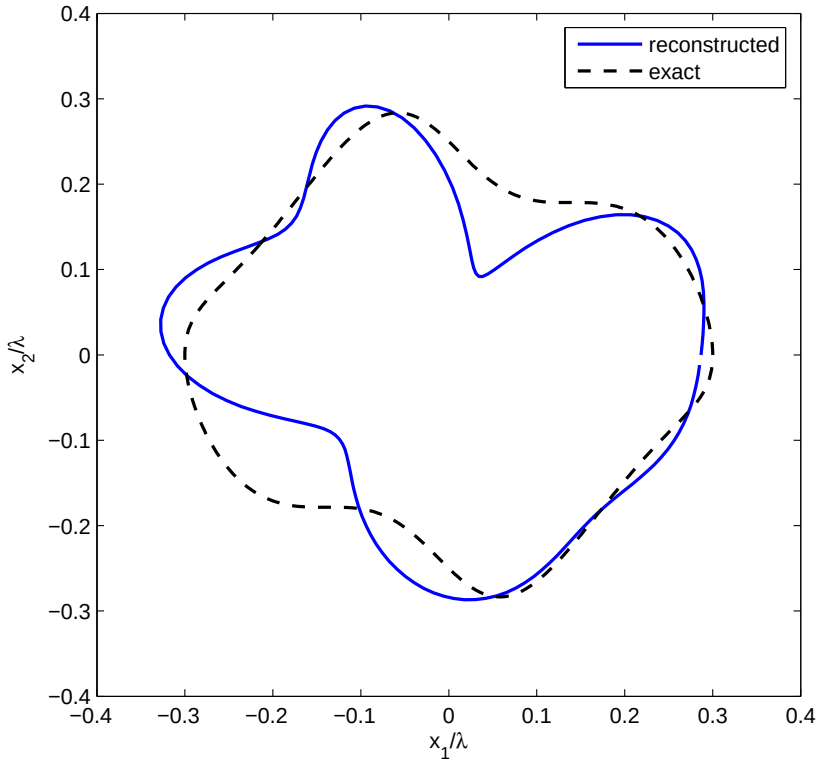

Figure 5.9: Exact and reconstructed geometries of a potato-shape object for the radius of the β is 25% greater than f_{max}

results if the radius of the β circle is at most 25% greater than the maximum radius of the object to be reconstructed.

5.5 Effect of The Conductivity of The Dielectric Cylinder

Since the absorbtion characteristics of the coating dielectric cylinder becomes significant as the conductivity increases, accordingly the reconstruction error is expected to increase. In this section effect of the conductivity of the coating cylinder is investigated. Permittivity and thickness of the dielectric cylinder is fixed at the values $\varepsilon_r = 4$ and $a = 0.4$, while the operating frequency is $300MHz$. Number of basis functions in the least square regularization is $Q = 8$. In addition, for the following two examples the incidence angle is set to $\phi_0 = \pi/4$ radian. Figures 5.10 and 5.11 shows that the method provides satisfactory results if the conductivity of the dielectric cylinder, namely σ is smaller than $0.1(S.m^{-1})$ for a thickness of 0.4λ. Reconstruction errors for Figures 5.10 and 5.11 are 7% and 15% respectively.

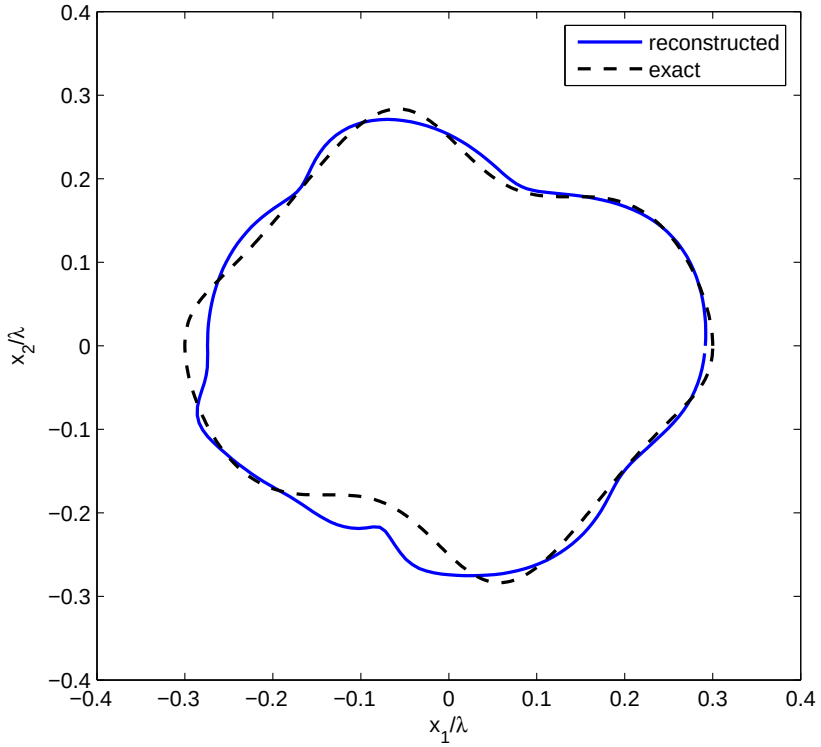

Figure 5.10: Exact and reconstructed geometries of a potato-shape object for $\sigma = 0.01(S.m^{-1})$

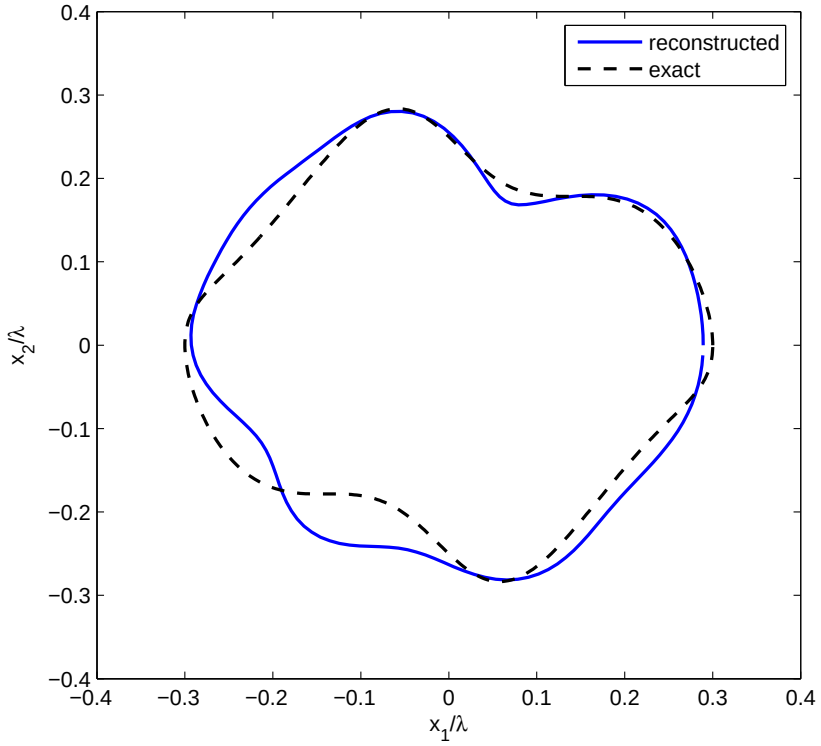

Figure 5.11: Exact and reconstructed geometries of a potato-shape object for $\sigma = 0.1(S.m^{-1})$

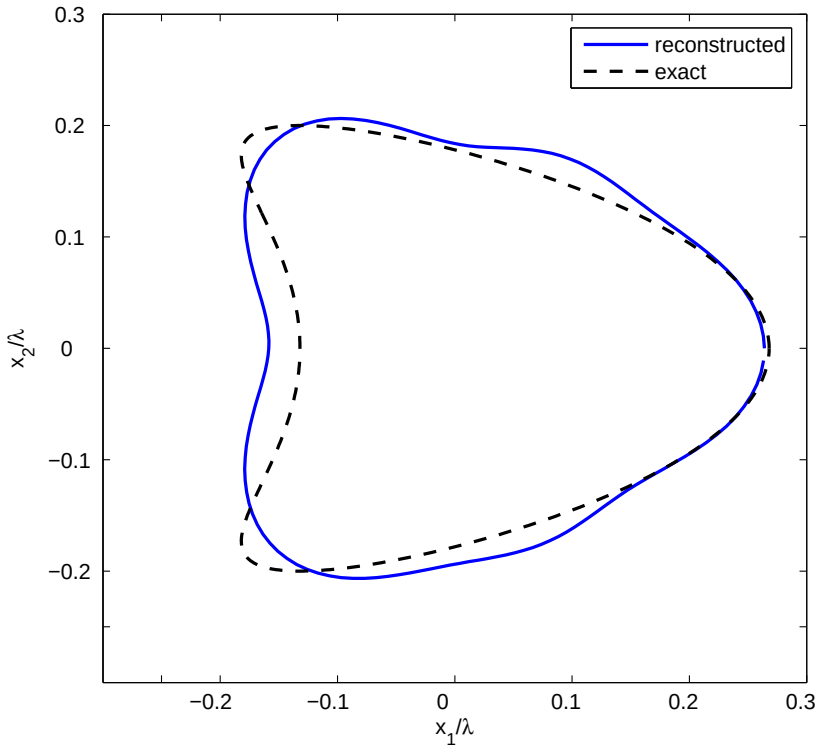

Figure 5.12: Exact and reconstructed geometries of a kite-shape object

5.6 Validation of The Method For Different Geometries

To show the validity of the method for different geometries a kite-shaped object with a radius of 0.27λ given by the parametric equation

$$x_1 = 0.2\cos\phi + 0.1\cos 2\phi - 0.032$$

$$x_2 = 0.2\sin\phi, \ \ \phi \in (0, 2\pi).$$

is considered. The object is buried in a dielectric cylinder with a radius of 0.35λ. Reconstruction is obtained for $\phi_0 = 180^\circ, \varepsilon_r = 4, \sigma = 10^{-2}(S.m^{-1})$ and $Q = 6$ basis functions are used in the least square regularization. Note that the incident field illuminates the target from the non-convex region of the object where a more erroneous reconstruction is expected to be achieved because of the smoothing effect of the introduced regularization. Reconstruction is achieved with an error of 12% is shown in Figure 5.12.

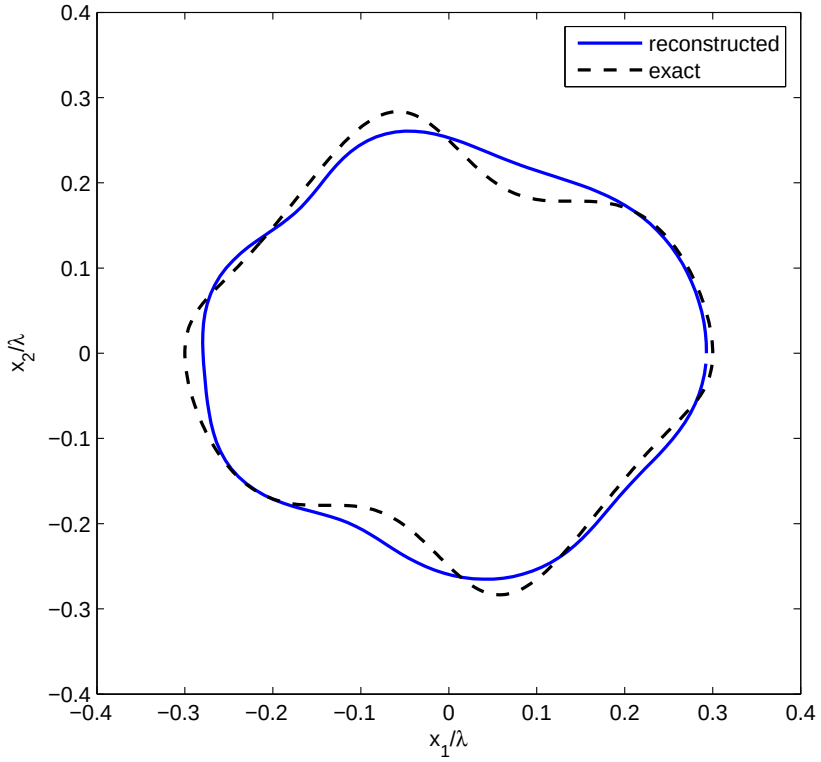

Figure 5.13: Exact and reconstructed geometries for single illumination

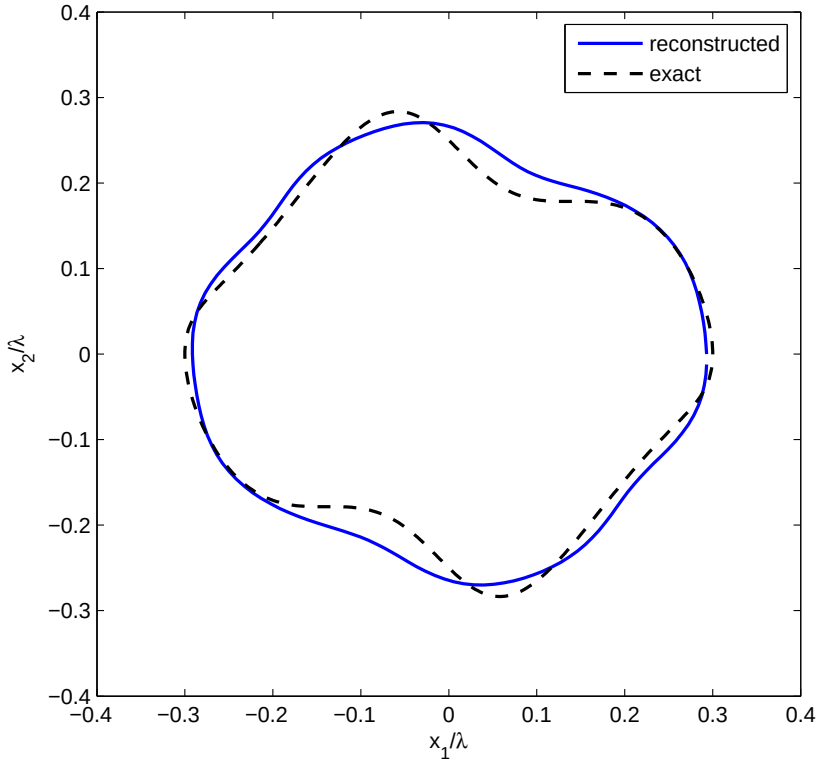

Figure 5.14: Exact and reconstructed geometries for two illuminations for $\phi_0 = \pi/4$ and $\phi_0 = 5\pi/4$

5.7 Enhanced Reconstruction Quality by The Use of Multiple Illuminations

The formulation of multiple illumination case of the method is given in Chapter 4. In this section examples are devoted to demonstrate the applicableness of the data obtained by multiple illuminations of the object. Results are obtained for a more contrast background namely, for $\varepsilon_r = 10$. Other parameters of the dielectric cylinder are $a = 0.4$ and $\sigma = 10^{-2}(S.m^{-1})$ where $Q = 6$.

It is observed that the use of multiple illuminations, provide slightly better reconstructions. The result in Figure 5.13 is more erroneous especially in the non-illuminated side compared to the one in Figure 5.14.

From the illustrative examples given above, one can conclude that the proposed method is capable of providing quite satisfactory reconstructions, even if data collected through a single illumination is used.

6. CONCLUSION

In the proposed thesis, a simple and effective method for the reconstruction of the shape of an inaccessible perfectly electric conducting target which is buried in a homogeneous dielectric cylinder, using a single and multiple illumination, single-frequency scattering experiment, is introduced.

The method consists of two parts: First, an approximation of the field on a circle, namely β circle, close to the minimum one covering the object is determined by means of a properly regularized single-layer potential approach outside the dielectric cylinder followed by Bessel series representation of the scattered field inside the dielectric cylinder. Then, a simple non-linear problem is solved to achieve the unknown boundary by minimizing a polynomial cost functional given by few terms of a Taylor expansion of the total field as function of the unknown surface profile. A detailed investigation of these parts are made in Chapter 2 and Chapter 3.

Two particular regularization scheme are applied to the overall inverse problem in order to obtain a robust algorithm to noisy data. Concerning the first part of the reconstruction algorithm, particular attention has been given in the solution of the ill-posed linear operator equation by using a Tikhonov regularization in such a way that the corresponding approximated near-field is as less sensitive as possible to errors on data. On the other hand, in the second part, the non-linear inversion, which is solved in the least square sense via the Newton method, is properly regularized through the use of a finite dimensional representation of the unknown contour. Despite the reduced amount of exploited data, the method yields to very accurate reconstructions of smooth shapes, provided that the size of the PEC object and the coating cylinder is comparable to the wavelength. Moreover, even when a single illumination is used, reasonably good estimations of the non-illuminated side of the targets are achieved. It should be noted that

the as the radius of the coating cylinder increase the method gives more erroneous results which is because Bessel series representation of the scattered field does not imply adequate information needed for proper reconstructions. It is remarkable that the method is simple and fast allowing to the results to be improved by using more tha one illuminations, without reducing its efficiency and simplicity. Interestingly, such an approach is almost straightforward as the unknown quantity does not depend on the incident field, which is instead the case that occurs in other approaches such as, for instance when the reconstruction is based on the Kirchhoff approximation [24, 27].

REFERENCES

[1] **Richmond, J.A.**, 1965. Scattering by a dielectric cylinder of arbitrary cross section shape, *IEEE Trans. Antennas and Propagatation*, **13**, 334–341.

[2] **Rao, S.**, **Wilton, D. and Glisson, A.**, 1982. Electromagnetic Scattering By Surfaces Of Arbitrary Shape, *IEEE Trans. Antennas and Propagatation*, **30**, 409–418.

[3] **Ishimaru, A.**, 1991. Electromagnetic Wave Propagation, Radiation, and Scattering, Prentice Hall, New Jersey.

[4] **Felsen, L.B. and Marcuvitz, N.**, 1994. Radiation and Scattering of Waves, Wiley-IEEE Press, New Jersey.

[5] **Bowman, J.J.**, **Senior, T.B.A. and Uslenghi, P.L.E.**, 1969. Electromagnetic and Acoustic Scattering by Simple Shapes, Hemisphere Publishing Corp., New York.

[6] **Paolini, F.J.**, 1987. Implementation of microwave diffraction tomography for measurement of dielectric constant distribution, *Microwave Opt. Antennas*, **134**, 25–29.

[7] **Bolomey, J.C.**, **Izadnegahdar, A.**, **Jofre, L.**, **Pichot, C.**, **Peronnet, G. and Solaimani, M.**, 1982. Microwave diffraction tomography for biomedical applications, *IEEE Trans. Microwave Theory Tech.*, **30**, 1998–2000,.

[8] **Tabbara, W.**, **Duchine, B.**, **Pichot, C.**, **Lesselier, D.**, **Chommeloux, L. and Joachimowicz, N.**, 1988. Diffraction tomography: Contribution to the analysis of some applications in microwaves and ultrasonics, *Inverse Problems*, **4**, 305–331.

[9] **Bolomey, J.C. and Pichot, C.**, 1990. Microwave tomography: From theory to practical imaging systems, *Int. J. Imag. Syst. Tech.*, **1**, 119–131.

[10] **Wang, Y.M. and Chew, W.C.**, 1989. An iterative solution of two-dimensional electromagnetic inverse scattering problem, *Int. J. Imag. Syst. Tech.*, **1**, 100– 108.

[11] **Caorsi, S.**, **Massa, A.**, **Pastorino, M. and Donelli, M.**, 2004. Improved microwave imaging procedure for non-destructive evaluations of two-dimensional structures, *IEEE Trans. on Antennas and Propagation*, **52**, 1386–1397.

[12] **Benedetti, M.**, **Donelli, M. and Massa, A.**, 2007. Multicrack Detection in Two-Dimensional Structures by Means of GA-Based Strategies, *IEEE Trans. on Antennas and Propagation*, **55**, 205–215.

[13] **Qing, A.**, 2003. Electromagnetic Inverse Scattering of Multiple Two-Dimensional Perfectly Conducting Objects by the Differential Evolution Strategy, *IEEE Trans. on Antennas and Propagation*, **51**, 1251–1263.

[14] **Qing, A.**, **Lee, C.K. and Jen, L.**, 2001. Electromagnetic inverse scattering of two-dimensional perfectly conducting objects by real-coded geneticalgorithm, *IEEE Trans. Geoscience and Remote Sensing*, **39**, 665–676.

[15] **Buyukozturk, O. and Rhim, H.**, 1997. Radar imaging of concrete specimens for nondestructive testing, *Consturction and building materials*, **11**, 195–198.

[16] **Caorsi, S. and Pastorino, M.**, 1998. Microwave imaging using a genetic algorithm, *Electromagnetic Nondestructive Evaluation (II)*, **14**, 233–242.

[17] **Pastorino, M.**, **Massa, A. and Caorsi, S.**, 2000. A microwave inverse scattering technique for image reconstruction based on a genetic algorithm, *IEEE Trans. on Instrumentation and Measurement*, **49**, 573–578.

[18] **Weile, D. and Michielssen, E.**, 1997. Genetic algorithm optimization applied to electromagnetics: A review, *IEEE Trans. on Antennas and Propagation*, **45**, 243–253.

[19] **Colton, D. and Kirsh, A.**, 1996. A simple method for solving inverse scattering problems in the resonance regions, *Inverse Problems*, **13**, 383–393.

[20] **Colton, D. and Monk, P.**, 1998. A linear sampling method for the detection of leukemia using microwaves, *SIAM Journal of Appl. Math.*, **58**, 926–941.

[21] **Brühl, M. and Hanke, M.**, 2000. Numerical implementation of two noniterative methods for locating inclusions by impedance tomography, *Inverse Problems*, **16**, 1029–1042.

[22] **Charalambopoulos, A.**, **Gintides, D. and Kiriaki, K.**, 2002. Numerical implementation of two noniterative methods for locating inclusions by impedance tomography, *Inverse Problems*, **18**, 547–558.

[23] **Colton, D.**, **Coyle, J. and Monk, P.**, 2000. Recent developments in inverse acoustic scattering theory, *SIAM Rev.*, **42**, 369–414.

[24] **Bojarski, N.N.**, 1982. A survey of the physical optics inverse scattering identity, *IEEE Trans. Antennas and Propagat.*, **30**, 980–989.

[25] **Liu, N.Y. and Kiang, Y.W.**, 1996. Inverse scattering for conductors by the equivalent source method, *IEEE Trans. Antennas and Propagat.*, **44**, 310–316.

[26] **Belkebir, K.**, **Kleinmann, R.E. and Pichot, C.**, 1997. Microwave imaging-location and shape reconstruction from multifrequency scattering data, *IEEE Trans. Microwave Theory and Tech.*, **45**, 469–476.

[27] **Pierri, R.**, **Liseno, A. and Soldovieri, F.**, 2001. Shape reconstruction from PO multifrequency scattered fields via the singular value decomposition approach, *IEEE Trans. Antennas and Propagat.*, **49**, 1333–1343.

[28] **Roger, A.**, 1981. Newton-Kantorovitch algorithm applied to an electromagnetic inverse problem, *IEEE Trans. Antennas Propagat*, **29**, 231–238.

[29] **Chiu, C.C. and Kiang, Y.W.**, 1992. Electromagnetic Inverse Scattering of a Conducting Cylinder Buried in a Lossy Half-space, *IEEE Trans. Antennas Propagat.*, **40**, 1562–1566.

[30] **Firoozobadi, R.**, **Miller, E.L.**, **Rappaport, C.M. and Morgenthaler, A.W.**, 2007. Subsurface Sensing of Buried Objects Under a Randomly Rough Surface Using Scattered Electromagnetic Field Data, *IEEE Trans. Geosci. Remote Sens.*, **45**, 104–118.

[31] **Chiu, C.C.**, 1998. Inverse Scattering of Inhomogeneous Biaxial Materials Coated on a Conductor, *IEEE Trans. Antennas Propagat.*, **46**, 218–226.

[32] **Chiu, C.C.**, 2005. Image Reconstruction of Buried Dielectric Cylinders Coated on a Conductor by TE Wave Illumination, *Taylor and Francis Electromagnetics*, **25**, 427–441.

[33] **Colton, D. and Kress, R.**, 1999. Inverse Acoustic and Electromagnetic Scattering Theory, Springer-Verlag, Berlin.

[34] **Bertero, M.**, 1989. Linear inverse and ill-posed problems, *Adv. Electron Phys.*, **75**, 1–120.

[35] **Akduman, I.**, **Kress, R. and Yapar, A.**, 2006. Iterative Reconstruction of Dielectric Rough Surface Profiles at Fixed Frequency, *Inverse Problems*, **22**, 939–954.

[36] **Soldovieri, F.**, **Brancaccio, A.**, **Leone, G. and Pierri, R.**, 2005. Shape Reconstruction of Perfectly Conducting Objects By Multiview Experimental Data, *IEEE Trans. Geosci. Remote Sens.*, **43**, 65–71.

CIRCULUM VITAE

Oğuz Semerci was born in Ankara, Turkey in 1983. He received his B.Sc. degree in Telecommunication Engineering from İstanbul Technical University in 2006. Since 2006, he is working towards M.Sc. degree in Telecommunications Engineering program of Institute of Science and Technology at İstanbul Technical University. Currently, he is serving as a research assistant at Electromagnetic Fields and Microwave Technique Division of İstanbul Technical University.